3

Cooling curve prediction for controlled unidirectional solidification under influence of shrinkage: semi-analytical approach

3.1 INTRODUCTION

Quality of casting products can be significantly improved by controlling the crystal growth rate. Both dendritic and equiaxed grain structures depend strongly on crystal growth rate along the crystallographic direction. Uncontrolled solidification processes may lead to the formation of porous and columnar material with an extremely non-homogeneous composition distribution. These undesirable micro-structures can be avoided by adopting an optimal cooling rate (K/s) during the crystal growth. The present work focuses on determining suitable cooling curves to obtain desired unidirectional crystal growth rates, by implementing a semi-analytical model. Here, cooling curve as the time history of temperature evolution at the cold boundary. The proposed semi-analytical heat transfer model is diffusion driven, and, accounts for shrinkage effect during solidification.

Directional single crystal growth has many applications related to production of high frequency turbine blades, solar absorber materials, photovoltaic materials, and many more. Crystal growth is the fundamental phenomenon that defines the grain structure during solidification processes. Favourable mechanical properties such as strength and hardness of cast products can be achieved by controlling grain structure [Gokhale and Patel, 2005; Lopez et al., 2003; Hemanth, 1999]. Attempts have been made to refine micro-structure of castings by adding refiner and modifier to the melt, in order to improve the mechanical strength of cast products [Liao et al., 2002]. One of the most important factors that influence the growth of micro-structure is the cooling rate (K/s) [Zhuang and Langer, 1989; Zhang et al., 2000, 2008]. Zhuang and Langer [1989] achieved fine equiaxed grain structure of Co-Cr-Mo alloys by employing fast cooling rate during casting. Zhang et al. [2008] studied a fast cooling technology using a copper mold for solidification of Al356 alloy. Hosseini et al. [2013] also studied the effect of cooling rate on mechanical properties, solidification parameters and micro-structures of LM13 alloy. Zhang et al. [2008] and Hosseini et al. [2013] concluded that higher cooling rate and shorter solidification time causes further refinement of micro-structures, resulting segregation-free micro-structures with homogeneous distribution of micro-porosity. Boettinger et al. [1984] reported prevalence of conventional dendritic or eutectic structures at low crystal growth rate condition. Boettinger et al. [1984] also suggested the possibility of obtaining micro-segregation-free single phase structures at higher crystal growth rates. Sarreal and Abbaschian [1986] and Taha et al. [2002] reported existence of optimal cooling rate for achieving maximum amount of non-equilibrium eutectic (NEE) phase in the directionally solidified sample of non-eutectic alloys. Sarreal and Abbaschian [1986] and Taha et al. [2002] interpreted this phenomenon as a result of back diffusion, dendrite tip under-cooling, and eutectic temperature depression. Eskin et al. [2005] and Du et al. [2007] studied the effect of cooling rate on non-eutectic Al-Cu alloy casts, and made similar conclusion on the existence of an optimum cooling rate. Kasperovich et al. [2008] investigated non-eutectic Al-Cu alloy solidification under the large range of cooling rates (0.01-20000 K/s) to conclude the similar trend. Kasperovich et al. [2008] also used 2-D pseudo-front tracking (PFT) model developed by Du and Jacot [2005] to

predict the eutectic fractions, and validated the numerical results with experimental data.

Uncontrolled cooling rate causes inhomogeneous distribution of grain-size and micro-porosity which may lead to severe casting defects [Zhang et al., 2008; Hosseini et al., 2013]. Challenge of determining appropriate cooling curve to ensure desired crystal growth rate received considerable attention from several research groups [Dorschu, 1968; Mullin and Nỳvlt, 1971; Lukens et al., 1981; Gandin, 2000b,a; Alkemper et al., 1998]. The experimental investigation by Dorschu [1968] involves controlling the cooling rate during gas metal arc welding process. Mullin and Nỳvlt [1971] presented a mathematical model to predict cooling curves based on data measured during crystallization process. Lukens et al. [1981] monitored the cooling rate of the weld metal by means of infrared technique in order to study micro-structures near the weld bead. Gandin [2000b,a] described a 1-D heat flow model to study uni-directional solidification of pure Al and Al-Si alloy. Gandin [2000b,a] determined the interface velocity using experimentally obtained cooling curves incorporating the shrinkage effect. Alkemper et al. [1998] described a simple control of solidification parameters like velocity, and temperature gradient of the melt during an experimental study involving unidirectional solidification of Al-Si alloy.

The procedure of predicting the solid-liquid interface velocities, and the effect of crystal growth rate on micro-structures are abundant in literature [Gokhale and Patel, 2005; Lopez et al., 2003; Hemanth, 1999; Liao et al., 2002; Zhuang and Langer, 1989; Zhang et al., 2000, 2008; Hosseini et al., 2013; Boettinger et al., 1984; Sarreal and Abbaschian, 1986; Taha et al., 2002; Eskin et al., 2005; Du et al., 2007; Kasperovich et al., 2008; Du and Jacot, 2005; Dorschu, 1968; Mullin and Nỳvlt, 1971; Lukens et al., 1981; Gandin, 2000b,a; Alkemper et al., 1998]. However, the prediction of appropriate cooling curve to obtain desired crystal growth rate considering shrinkage effect is hardly investigated. There exists a visible gap in the research area associated with theoretical prediction of cooling curve to attain controlled crystal growth. All the existing solidification models deal with solving forward problems, where solid-liquid interface growth and temperature evolution of the domain is obtained for prescribed boundary conditions (namely Dirichlet, Neumann, and, mixed boundary conditions). The present study aims to develop a model which is capable of solving inverse problem. The inverse problem deals with determining suitable temperature evolution at the cold boundary to obtain prescribed unidirectional crystal growth rate. The proposed model accounts for shrinkage effect, and capable of predicting cooling curve during complete solidification of a melt sample of finite length. The cooling curve prediction by the model is validated by using it as the transient boundary condition for an existing enthalpy updating scheme based numerical model. The proposed model is also applied to empirical data reported in literature, to validate the model against experimental results. All the validations showcased excellent fit. The proposed model will facilitate controlled unidirectional crystal growth rate by providing cooling rate (K/s) as an input for the experiments involving directional solidification.

3.2 MATHEMATICAL MODEL

Diverse directional solidification processes like Bridgman technique [Bridgman, 1931], high rate solidification (HRS) [Tingquist and Laux, 1974], liquid-metal cooling (LMC) [Giamei and Tschinkel, 1976], and vertical gradient freeze (VGF) [Das et al., 2013] methods have been employed by several research groups to acquire single crystal growth. Bridgman technique [Bridgman, 1931] pioneers among all the existing directional solidification methods [Bridgman, 1931; Tingquist and Laux, 1974; Giamei and Tschinkel, 1976; Das et al., 2013], and, most of the directional solidification studies are associated with this technique.

The Bridgman technique [Bridgman, 1931] involves slow pulling of the liquid melt through differentially heated zones. The upper and lower zones are maintained above and below the melting point temperature of the sample material respectively. A thermal insulation separates

the upper hot zone from the lower cold zone. The crystal growth rate in Bridgman technique [Bridgman, 1931] coincides with the pulling speed of the melt through the differentially heated zones. One can overcome the complications associated with the melt pulling in Bridgman technique by imposing suitable cooling rate at the two ends of a fixed immobile melt sample [Gandin, 2000b,a; Alkemper et al., 1998]. The key to control the directional crystal growth rate from fixed immobile melt sample is finding the appropriate time dependent heat flux conditions at the melt boundaries. For directional solidification of pure metal or eutectic alloy, the temperature of the crystal growth front (solid-liquid interface) always remains at freezing point (T_m for pure metal) or eutectic temperature (T_e for eutectic alloys). The evolution of the length of solid phase (distance between the solid-liquid interface and the cold end: $L_s(t) = \int_0^t v_i dt$) can be easily obtained from the desired crystal growth rate (v_i). Therefore, the time dependent heat flux $q_c''(t)$ to control the crystal growth rate essentially depends on the temperature evolution at the cold end (Since, $q_c''(t) = k_s[T_m - T_c(0,t)]/L_s(t)$). So, we can conclude, that obtaining controlled single crystal growth from an immobile melt sample of fixed length akin to Bridgman method has a strong dependence on the successful prediction of cooling curve: $T_c(0,t)$.

The domain of interest for present problem under consideration is same as shown in figure 2.1. Once again the domain addresses directional solidification of metals with shrinkage. The bottom cooling configuration and the high slenderness ratio (l/d) of the cavity ensures complete suppression of free convection thus, heat transfer is purely diffusion driven. Similar assumptions for the model were considered as discussed for the previous problem. The present study deals with predicting the suitable transient cold temperature boundary condition ($T(0,t) = T_c(0,t)$) for a prescribed growth rate of interface $dx_i/dt = v_i^{desired}$ or $f(t)$.

A domain filled with liquid melt maintained at a temperature T_i above the melting point (T_m) is the initial condition. The cooling ensues by reducing temperature of the bottom end of the cavity at a constant rate ($\partial T_c/\partial t = C_r$) until the bottom end reaches melting temperature (T_m). The cold boundary temperature varies as $T_c(0,t) = T_i - C_r t$ (till $T_c(0,t) = T_m$), which is a time dependent Dirichlet type boundary condition. For the present study, a time step based approach with time averaged constant temperature boundary condition is used for each time step (Δt) [Chakraborty et al., 2017]. The time averaged temperature of cold boundary $T_c^{(k)}$ during a given time step $\Delta t^{(k)}$ can be shown to be $T_c^{(k)} = T_c^{(k-1)} - C_r(\Delta t^{(k)} + \Delta t^{(k-1)})/2$. With this time averaged temperature boundary condition, temperature distribution in the liquid domain prior to onset of solidification can be expressed after (k)th time step as,

$$T_l^{(k)} = T_c^{(k)} + \sum_{n=1}^{\infty} \exp\left(\frac{-\alpha_l(2n-1)^2\pi^2\Delta t^{(k)}}{4L_0^2}\right) \sin\left(\frac{(2n-1)\pi x}{2L_0}\right) G_n^{(k)} \quad 0 \leqslant x \leqslant L_0 \tag{3.1}$$

G_n appearing in Eq. 3.1 is calculated from orthogonality condition. G_n depends on temperature distribution obtained at the previous time step $\Delta t^{(k-1)}$ and is expressed as follows,

$$G_n^{(k)} = \frac{2C_r(\Delta t^{(k)} + \Delta t^{(k-1)})}{(2n-1)\pi} + \exp\left(\frac{-\alpha_l(2n-1)^2\pi^2\Delta t^{(k-1)}}{4L_0^2}\right) G_n^{(k-1)} \tag{3.2}$$

Where, $G_n^{(1)} = 2C_r\Delta t^{(1)}/(2n-1)\pi$, and L_0 is the initial length of the liquid domain before the onset of solidification.

Once, $T_c(0,t) = T_m$, a ND approach is implemented for the further derivation of solidification model. The governing Eq. 2.1-2.3 are obtained in dimensionless form considering ND temperature $\theta_\phi = (T_i - T_\phi)/(T_i - T_c(0,t))$, ND distance $X = x/L_0$ and ND time $F_o = \alpha_l t/L_0^2$ (Fourier Number), and are given as follows.

$$\frac{\partial \theta_\phi}{\partial F_o} = \alpha_\phi^* \frac{\partial^2 \theta_\phi}{\partial X^2} \tag{3.3}$$

$$\frac{dX_i^*}{dF_o} = -\frac{\beta_s \alpha_s^*}{\theta_m} \left.\frac{\partial \theta_s}{\partial X}\right|_{X_i^*} + \frac{\beta_l \alpha_l^*}{\theta_m} \left.\frac{\partial \theta_l}{\partial X}\right|_{X_i^*} \tag{3.4}$$

$$L^{*(k)} = L^{*(k-1)} + \left(1 - \frac{\rho_s}{\rho_l}\right)\left(X_i^{*(k)} - X_i^{*(k-1)}\right) \tag{3.5}$$

If the ND interface location is defined as $X_i^*(F_o) = x_i(t)/L_0$ and the ND overall length is defined as $L^*(F_o) = L(t)/L_0$, then the modified boundary conditions pertaining to solid domain for the subsequent time-steps can be written as: $\theta_s(0, F_o) = 1$ and $\theta_s(X_i^*, F_o) = \theta_m(F_o)$. Where, $\theta_m(F_o)$ is defined as $(T_i - T_m)/(T_i - T_c(0,t))$. Similarly for the liquid domain, the boundary conditions are defined as $\theta_l(X_i^*, F_o) = \theta_m(F_o)$ and $\partial\theta_l/\partial X|_{X=L^*} = 0$.

$\beta_{\phi=s,l}$ and $\alpha_{\phi=s,l}$ appearing in dimensionless Stefan condition (Eq. 3.4) at the interface are defined as: $\beta_\phi = \rho_\phi c_{p\phi}(T_i - T_m)/\rho_s h_{sl}$ and $\alpha_\phi^* = \alpha_\phi/\alpha_l$. For prescribed crystal growth rate, dX_i^*/dF_o appearing in Eq. 3.4 is a constant value.

Time step based treatment of initial condition proposed by Chakraborty et al. [2017] is adopted to solve Eq. 3.3-3.5. The solution of the previous time-step is used as the initial condition for the current time-step. The system of equations described by Eq. 3.3-3.5 needs to be solved simultaneously to obtain θ_ϕ profile. The analytical solution of heat diffusion Eq. 3.3 for solid and liquid domains for the present ND time-step ($\Delta F_o^{(k)}$) can be written as:

$$\theta_s^{(k)} = 1 + \frac{(\theta_m^{(k)} - 1)X}{X_i^{*(k)}} + \sum_{n=1}^{\infty} \exp\left(\frac{-\alpha_s^* n^2 \pi^2 \Delta F_o^{(k)}}{X_i^{*(k)2}}\right) \sin\left(\frac{n\pi X}{X_i^{*(k)}}\right) C_n^{(k)} \qquad 0 \leqslant X \leqslant X_i^{*(k)} \tag{3.6}$$

$$\theta_l^{(k)} = \theta_m^{(k)} + \sum_{n=1}^{\infty} \exp\left(\frac{-(2n-1)^2 \pi^2 \Delta F_o^{(k)}}{4\left(L^{*(k)} - X_i^{*(k)}\right)^2}\right) \sin\left(\frac{(2n-1)\pi\left(X - X_i^{*(k)}\right)}{2\left(L^{*(k)} - X_i^{*(k)}\right)}\right) D_n^{(k)}$$

$$X_i^{*(k)} \leqslant X \leqslant L^{*(k)} \tag{3.7}$$

Where, $\theta_{\phi=s,l}^{(k)}$ represents ND temperature distribution in the solid and liquid domain at (k)th time step. During each time steps, the temperature at the cold boundary is considered to be having a time averaged constant value over the duration of the corresponding time-step. This time averaged temperature keeps decreasing for each successive time steps. The ND interface location ($X_i^{*(k)}$) appearing in Eq. 3.6-Eq. 3.7, is specified by the desired crystal growth rate or interface velocity. C_n and D_n appearing in Eq. 3.6 and Eq. 3.7 arise from the orthogonality condition. They depend on ND temperature distributions in solid and liquid domain, obtained at the previous ND time step $\Delta F_o^{(k-1)}$.

$$C_n^{(k)} = \frac{2}{X_i^{*(k-1)}} \int_0^{X_i^{*(k-1)}} \left(\theta_s^{(k-1)} - \frac{\left(\theta_m^{(k-1)} - 1\right)X}{X_i^{*(k-1)}} - 1\right) \sin\left(\frac{n\pi X}{X_i^{*(k-1)}}\right) dX \tag{3.8}$$

$$D_n^{(k)} = \frac{2}{\left(L^{*(k-1)} - X_i^{*(k-1)}\right)} \int_{X_i^{*(k-1)}}^{L^{*(k-1)}} \left(\theta_l^{(k-1)} - \theta_m^{(k-1)}\right) \sin\left(\frac{(2n-1)\pi\left(X - X_i^{*(k-1)}\right)}{2\left(L^{*(k-1)} - X_i^{*(k-1)}\right)}\right) dX \tag{3.9}$$

$\theta_\phi^{(k-1)}$, $X_i^{*(k-1)}$ and $L^{*(k-1)}$ in Eq. 3.8 and Eq. 3.9 are obtained from the previous ND time step $\Delta F_o^{(k-1)}$.

The temperature distributions in the solid and liquid domains have been completely defined by Eq. 3.6-3.9. Finding the initial temperature distributions in the liquid region is trivial during onset of solidification. However, defining initial temperature distribution in the solid

region during the onset of solidification is challenging, as solid domain is yet to be evolved at this stage. By considering a very small time step ($\Delta t \sim 1\ \mu s$), a very small value of ND interface location ($X_i^* \to 0$) is attainable. All the exponential terms appearing in Eq. 3.6 tends to be zero as $\lim_{X_i^* \to 0}$, hence, $\theta_s \to 1 + (\theta_m - 1)X/X_i^*$. Therefore, for the first time-step during which the onset of solidification is considered, the temperature distribution simply becomes $\theta_s^{(1)} \approx 1 + (\theta_m^{(1)} - 1)X/X_i^{*(1)}$, provided the chosen time step is extremely small ($\Delta t \approx 1\ \mu s$). Thus, estimation of $C_n^{(1)}$ becomes redundant.

Another possible way of selecting $\theta_s^{(1)}$ after a very small time instant ($\Delta t \sim 1\ \mu s$) during the onset of solidification can be derived through the isothermal condition of the interface during liquid-solid phase transformation. Solid domain is extremely thin ($X_i^* \to 0$) during the onset of solidification. Therefore, the entire solid region except the cold boundary may be considered to be at freezing point (T_m) during the onset of solidification. The cold boundary however, is at a temperature $T_c(0,t) < T_m$ during this onset. From this definition $\theta_s^{(1)}(X)$ can be considered to be a step function, having a singularity at $X = 0$. The value of $\theta_s^{(1)}$ is unity at $X = 0$, and, it is θ_m everywhere else ($0 < X \leq X_i^{*(1)}$). Once again, the calculation of $C_n^{(1)}$ is redundant. Based on the above discussions, two alternative options of ND temperature distribution can be obtained during the onset of solidification. For a very small time-step ($\Delta t \sim 1\ \mu s$), two alternative $\theta_s^{(1)}$ profiles are expressed as follows.

$$\theta_s^{(1)} = 1 + (\theta_m^{(1)} - 1)X/X_i^{*(1)} \tag{3.10}$$

and,

$$\theta_s^{(1)} = \begin{cases} 1 & X = 0 \\ \theta_m^{(1)} & 0 < X \leq X_i^{*(1)} \end{cases} \tag{3.11}$$

The effect of these two alternatives initial solid temperature profiles on the final outcome of predicted cooling curve will be expounded further in the subsequent section.

The temperature distribution in the liquid domain θ_l can be calculated by using Eq. 3.7, 3.9, and 3.1. Substitution of θ_s and θ_l from Eq. 3.6 and 3.7 in Eq. 3.4 leads to the following expression.

$$\frac{dX_i^*}{dF_o} = \frac{\beta_s \alpha_s^* (1 - \theta_m^{(k)})}{\theta_m^{(k)} X_i^{*(k)}} - \frac{\beta_s \alpha_s^*}{\theta_m^{(k)} X_i^{*(k)}} \sum_{n=1}^{\infty} (-1)^n n\pi \exp\left(\frac{-\alpha_s^* n^2 \pi^2 \Delta F_o^{(k)}}{X_i^{*(k)2}}\right) C_n^{(k)} + \frac{\beta_l \alpha_l^*}{\theta_m^{(k)} (L^{*(k)} - X_i^{*(k)})} \sum_{n=1}^{\infty} \frac{(2n-1)\pi}{2} \exp\left(\frac{-(2n-1)^2 \pi^2 \Delta F_o^{(k)}}{4(L^{*(k)} - X_i^{*(k)})^2}\right) D_n^{(k)} \tag{3.12}$$

In the above formulation, $\theta_m(F_o)$ is the only unknown. The interface growth rate (dX_i^*/dF_o) is known in terms of desired crystal growth rate. Since, $\theta_m(F_o)$ is defined as $(T_i - T_m)/(T_i - T_c(0,t))$. By finding the solution for $\theta_m(F_o)$ from Eq. 3.12, we can evaluate $T_c(0,t)$. In order to solve unknown $\theta_m(F_o)$ from Eq. 3.12, a simple semi-analytical scheme is applied as described in following steps.

1. Solidification starts, as $T_c(0,t)$ reaches below the melting temperature T_m and thus, θ_m=1 at $F_o = 0$ during the onset of solidification.

2. Consider a very small time-step ($\Delta t \sim 1\ \mu s$). Approximate temperature distribution in the solid from Eq. 3.10 or Eq. 3.11.

3. Obtain $D_n^{(1)}$ from Eq. 3.9 by calculating θ_l^0 from Eq. 3.1.

4. dX_i^*/dF_o appearing on the left hand side of Eq. 3.12 is known in terms of prescribed crystal growth rate or interface velocity U_i^*. Therefore, ND interface location ($X_i^{*(k)}$) can be easily comprehended as,

$$X_i^{*(k)} = X_i^{*(k-1)} + U_i^* \Delta F_o^{(k)} \tag{3.13}$$

After the very first time-step during the onset of solidification, the interface location must be $X_i^{*(1)} = U_i^* \Delta F_o^{(1)}$, as the initial interface location is $X_i^{*(0)} = 0$.

5. Evaluate $L^{*(1)}$ from Eq. 3.5.

6. All the parameters appearing in Eq. 3.12 are known except $\theta_m^{(1)}$. Replacing dX_i^*/dF_o with U_i^* and considering $C_n^{(1)} = 0$, two alternative formulations for $\theta_m^{(1)}$ can be obtained based on two alternative $\theta_s^{(1)}$ profiles (Eq. 3.10 and Eq. 3.11). The two alternative formulations to evaluate $\theta_m^{(1)}$ are as follows:

$$\theta_m^{(1)} = \frac{X_i^{*(1)}}{\left(U_i^* X_i^{*(1)} + \beta_s \alpha_s^*\right)} \left[\frac{\beta_s \alpha_s^*}{X_i^{*(1)}} + \frac{\beta_l \alpha_l^*}{(L^{*(1)} - X_i^{*(1)})} \sum_{n=1}^{\infty} \frac{(2n-1)\pi}{2} \exp\left(\frac{-(2n-1)^2 \pi^2 \Delta F_o^{(1)}}{4(L^{*(1)} - X_i^{*(1)})^2} \right) D_n^{(1)} \right] \tag{3.14}$$

and,

$$\theta_m^{(1)} = \frac{\beta_l \alpha_l^*}{U_i^* (L^{*(1)} - X_i^{*(1)})} \sum_{n=1}^{\infty} \frac{(2n-1)\pi}{2} \exp\left(\frac{-(2n-1)^2 \pi^2 \Delta F_o^{(1)}}{4(L^{*(1)} - X_i^{*(1)})^2} \right) D_n^{(1)} \tag{3.15}$$

7. Once $\theta_m^{(1)}$ is obtained from Eq. 3.14 or Eq. 3.15, calculate $T_c^{(1)}(t)$ from the definition of θ_m. Also, calculate ND temperature distribution in the solid domain ($\theta_s^{(1)}$) and liquid domains $\theta_l^{(1)}$ by substituting $\theta_m^{(1)}$ in Eq. 3.10 or 3.11 and Eq. 3.7 respectively.

8. The second time-step need not necessarily be a small time-step. Calculation of $C_n^{(2)}$ differs in a suggestive manner, depending upon which of the solid domain temperature profile is chosen (among Eq.3.10 and Eq.3.11) for the first time step. Substitution of Eq. 3.10 in Eq. 3.8 consistently produces $C_n^{(2)} = 0$, and maintains the unambiguous linear profile in the solid domain ($\theta_s^{(2)} = 1 + (\theta_m^{(2)} - 1) X / X_i^{*(2)}$). Choosing $\theta_s^{(1)}$ profile from Eq. 3.10 for the first time-step, perpetually renders $C_n^{(k)} = 0$ for all subsequent time-steps. Therefore, a linear temperature distribution is always maintained in the solid domain till the entire sample is solidified.

   On the other hand, substitution of Eq. 3.11 in Eq. 3.8 will require numerical integration of the right hand side of Eq. 3.8 in order to obtain $C_n^{(2)}$, as $\theta_s^{(1)}$ profile is a step function (Eq. 3.11). As far as the liquid domain is concerned, the substitution of $\theta_l^{(1)}$ profile in Eq. 3.9 will produce the following recursive formulation for $D_n^{(2)}$.

$$D_n^{(2)} = \exp\left(\frac{-(2n-1)^2 \pi^2 \Delta F_o^{(1)}}{4(L^{*(1)} - X_i^{*(1)})^2} \right) D_n^{(1)} \tag{3.16}$$

9. Obtain $X_i^{*(2)}$ and $L^{*(2)}$ from Eq. 3.13 and Eq. 3.5 respectively. Substitute $C_n^{(2)}$, $D_n^{(2)}$, $X_i^{*(2)}$, $L^{*(2)}$ and $dX_i^*/dF_o = U_i^*$ in Eq. 3.12 to calculate $\theta_m^{(2)}$ and hence, $T_c^{(2)}$.

10. For subsequent time-steps $C_n^{(k)}$ and $D_n^{(k)}$ can be calculated by direct substitution of Eq. 3.6 and 3.7 in Eq. 3.8 and 3.9 respectively. The substitutions leads to the following simplified recursive formulations for $C_n^{(k)}$ and $D_n^{(k)}$.

$$C_n^{(k)} = \begin{cases} 0 & \theta_s^{(1)} = 1 + (\theta_m^{(1)} - 1)X/X_i^{*(1)} \\ \exp\left(\frac{-\alpha_s^* n^2 \pi^2 \Delta F_o^{(k-1)}}{X_i^{*(k-1)^2}}\right) C_n^{(k-1)} & \theta_s^{(1)} = \theta_m^{(1)} \end{cases} \tag{3.17}$$

$$D_n^{(k)} = \exp\left(\frac{-(2n-1)^2 \pi^2 \Delta F_o^{(k-1)}}{4\left(L^{*(k-1)} - X_i^{*(k-1)}\right)^2}\right) D_n^{(k-1)} \tag{3.18}$$

11. Obtain $C_n^{(k)}$, $D_n^{(k)}$, $X_i^{*(k)}$, $L^{*(k)}$ from Eq. 3.17, 3.18, 3.13, and 3.5 respectively and, substitute them along with $dX_i^*/dF_o = U_i^*$ in Eq. 3.12 to evaluate $\theta_m^{(k)}$ and hence, $T_c^{(k)}$. Repeat steps 10 and 11 till the entire domain is solidified.

Steps 1-11 concludes the semi-analytical scheme to obtain the cooling curve $T_c(0,t)$, and temperature profile $T_\phi(x,t)$ during unidirectional solidification of a melt sample of finite length.

The incorporation of the shrinkage effect in the proposed model is limited to the bulk volume change (macroscopic) incurred by the reduction in the overall length of the domain due to solidification. However, from the micro-structure point of view, predominant effect of shrinkage is the formation of micro-porosity. For the present study, shrinkage induced micro-porosity has been neglected, which can be considered as a shortcoming of the proposed model.

3.3 VALIDATION AND CASE STUDIES

The semi-analytical model developed in the previous section postulates two alternative ND temperature profiles ($\theta_s^{(1)}$) within the solid region during the onset of solidification (Eq. 3.10 and Eq. 3.11). The influence of these two alternative temperature profiles is studied by comparing the predicted cooling curves obtained from these two formulations (Eq. 3.10 and Eq. 3.11). Cooling curves are predicted for unidirectional solidification of pure Al with prescribed crystal growth rate of $v_i = dx_i/dt = 100\ \mu m/s$. Shrinkage effect has been neglected for this preliminary analysis of the model. The thermo-physical properties of pure Al are considered to be: $k_l = 90\ W/mK$, $k_s = 350\ W/mK$, $c_{ps} = 875\ J/kgK$, $c_{pl} = 1250\ J/kgK$, $h_{sl} = 398\ kJ/kg$, and $T_m = 933.04\ K$. Initial temperature of the molten Al is considered to be $T_i = 939.84\ K$. Length of the domain is taken to be $L(t) = 100\ mm$. The cooling rate till the cold boundary reaches melting point (T_m) is chosen to be $C_r = 0.02\ K/s$. The temperature profile in the liquid domain is obtained using Eq. 3.1 till cold boundary temperature ($T_l(0,t)$) reaches melting temperature T_m. Once, cold boundary temperature reaches melting point ($T_l(0,t) = T_m$), steps 1-11 of the semi-analytical scheme are followed without implementing the shrinkage effect. Exclusion of shrinkage effect renders Eq. 2.3 and 3.5 to be redundant. L^* can be replaced by unity in Eq. 3.7, Eq. 3.9, Eq. 3.12, Eq. 3.14-3.16 and Eq. 3.18. The first time step during the onset of solidification has been considered to be 1 μs, and for the subsequent calculation, time step is chosen to be $\Delta t = 1\ s$. During the implementation of the scheme, the first cooling curve is predicted by using $\theta_s^{(1)}$ profile from Eq. 3.10. The second cooling curve is obtained by considering $\theta_s^{(1)}$ profile from Eq. 3.11.

Figure 3.1(a) shows the comparison of cooling curve obtained from these two alternative profile assumptions of ($\theta_s^{(1)}$). From figure 3.1(a), one can observe that both the profiles (Eq. 3.10 and Eq. 3.11) provide exactly identical cooling curves for the specified interface velocity. Therefore,

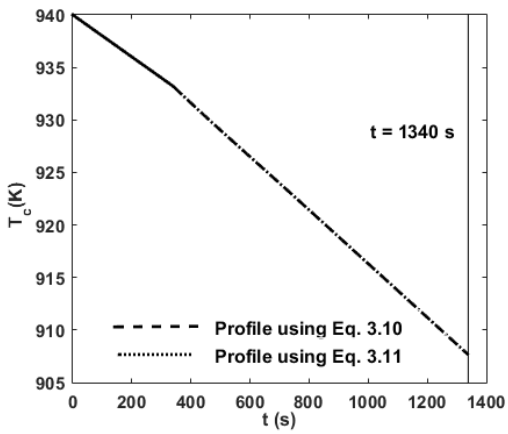

(a)

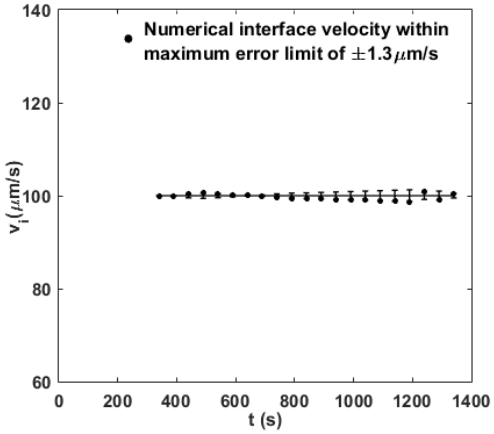

(b)

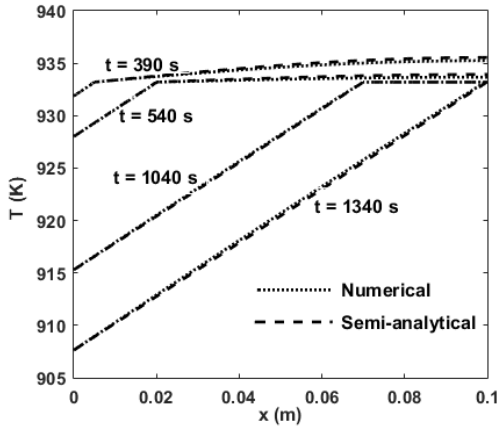

(c)

Figure 3.1 : (a) Effect of alternative $\theta_s^{(1)}$ profiles on cooling curves obtained during solidification of pure Al, (b) comparison of numerically obtained interface velocity with desired constant interface velocity v_i = 100 $\mu m/s$ based on which cooling curve is predicted, and (c) comparison between numerically and semi-analytically (proposed model) predicted temperature profiles along the solidifying Al melt sample at different time instants without considering shrinkage effect.

either of these two profiles can be considered as the initial temperature distribution within the solid phase during the onset of solidification. The exactly identical outcome from these two different profiles can be attributed to the extremely small first time step (1 μs). However, from the point of view of computational efforts, $\theta_s^{(1)}$ profile given by Eq. 3.10 is much more advantageous as compared to the $\theta_s^{(1)}$ profile given by Eq. 3.11. Profile assumption by Eq. 3.10 renders calculation of $C_n^{(k)}$(Eq. 3.8) to be perpetually redundant. Eq. 3.6 with $C_n^{(k)} = 0$ appears to be time independent. However, a close look at Eq. 3.6 reveals both $\theta_m^{(k)}$ and $X_i^{*(k)}$ are time dependent, hence $\theta_s^{(k)}$ is bound to be time dependent.

The proposed semi-analytical model is validated in four different manners. The first validation involves studying unidirectional solidification of pure Al with constant crystal growth rate. Shrinkage effect is not considered (*i.e.* $\rho_l = \rho_s = 2250\ kg/m^3$) for this first case study. The second, third and fourth validations (all validations are associated with solidification of pure Al) aim at testing the reliability of the cooling curve prediction from the model, when shrinkage effect is considered.

The second validation involves solving inverse (evaluation of cooling curve for specified interface growth rate) and forward (evaluation of interface growth rate from the cooling curve obtained by solving of the inverse problem) problems associated with unidirectional constant crystal growth rate. The third validation aims at addressing time-varying crystal growth rate by solving inverse and forward problems. The fourth and final validation involves comparison of predicted cooling curve from the proposed model with experimentally measured cooling curve reported by Gandin [2000b]. The reported crystal growth rate of pure Al by Gandin [2000b] was found out to be time dependent.

The first validation involves the following steps: (i) cooling curve is obtained (figure 3.1(a)) from the proposed model for a predefined constant unidirectional crystal growth rate of 100 $\mu m/s$. (ii) Crystal growth rate and temperature distribution is re-evaluated during solidification of the same sample from another well-established enthalpy updating scheme based numerical model [Voller et al., 1987; Brent et al., 1988; Chakraborty, 2017] with $T_c(0,t)$ as boundary condition. (iv) The re-evaluated crystal growth rate from the numerical model [Voller et al., 1987; Brent et al., 1988; Chakraborty, 2017] is compared with the input crystal growth rate to the proposed model (for predicting $T_c(0,t)$). If the predicted $T_c(0,t)$ from the proposed model is correct, then these two growth rates must closely match. Similarly, the temperature distributions obtained from the inverse (obtaining cooling curve for prescribed crystal growth rate) and forward (obtaining crystal growth rate from prescribed cooling curve) problems must be identical.

The proposed semi-analytical model is self-sufficient to solve both inverse and forward problems, and is capable to attain self-validate. However, in order to obtain wider acceptability of the proposed model, the forward problem is solved by using an existing finite volume based numerical model involving enthalpy updating scheme [Voller et al., 1987; Brent et al., 1988; Chakraborty, 2017]. The enthalpy updating scheme based numerical model [Voller et al., 1987; Brent et al., 1988; Chakraborty, 2017] under consideration is inadequate to address shrinkage effect. Therefore, cooling curve obtained from the present model is validated for its legitimacy, without considering the effect of shrinkage. The numerical model is based on a volume averaged energy equation (Eq. 2.18) [Chakraborty, 2017] and is capable of solving transient temperature distribution and solid-liquid interface location during the unidirectional solidification of a melt sample.

Figure 3.1(b) shows time evolution of interface velocity obtained by solving numerical model (Eq. 2.18) proposed by Chakraborty [2017]. Cooling curve ($T_c(0,t)$) shown in figure 3.1(a) is used as the cold boundary condition to solve Eq. 2.18. The cooling curve shown in figure 3.1(a), have two distinct trends before and after the onset of solidification. The first part of cooling curve before the onset of solidification is define by $T_c(0,t) = T_i - C_r t$, with $T_i = 939.84\ K$ and $C_r = 0.02\ K/s$. The second part of predicted cooling curve (figure 3.1(a)) is approximated by Gaussian fitting (with maximum RMS error $\mathcal{O} \sim 10^{-5}$). The Gaussian fitting is given as follows,

$$T_c(0,t) = \sum_{n=1}^{5} a_n exp\left(\left(-\frac{(t-b_n)}{c_n}\right)^2\right) \tag{3.19}$$

Where, $a_1 = 966.5$, $a_2 = 30.62$, $a_3 = -1.277$, $a_4 = 0.5712$, $a_5 = 0.0004776$, $b_1 = -2224$, $b_2 = 2372$, $b_3 = 148.4$, $b_4 = 236.7$, $b_5 = 854.1$, $c_1 = 11720$, $c_2 = 1391$, $c_3 = 372.8$, $c_4 = 295.2$, $c_5 = 88.84$. From figure 3.1(b), it can be observed that the solid-liquid interface velocity (v_i) obtained from the numerical model [Voller et al., 1987; Brent et al., 1988; Chakraborty, 2017], closely approximates to 100 $\mu m/s$ with a maximum error of $\pm 1.3\ \mu m/s$. Therefore, the validation of the cooling curve can be considered to be satisfactory. Figure 3.1(c) shows comparison of the temperature distribution along the solidifying melt sample, obtained at different time instants from the proposed model and the referred numerical model [Voller et al., 1987; Brent et al., 1988; Chakraborty, 2017]. Good agreement between the temperature profiles obtained from these two models can be clearly observed.

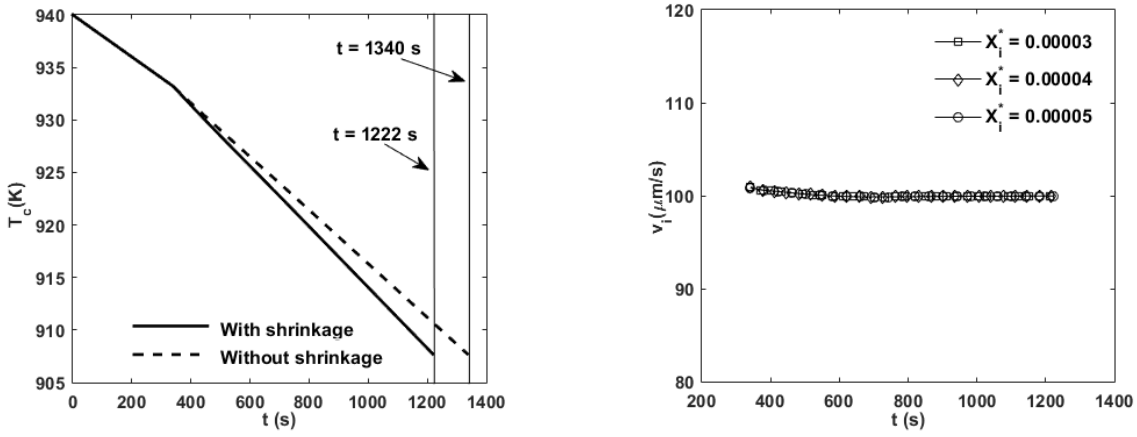

(a) (b)

Figure 3.2 : (a) Cooling curves with and without shrinkage effect for Al for constant interface growth velocity of 100 $\mu m/s$, and initial liquid domain length of 100 mm, and (b) validation of interface velocity obtained from the forward model with different guessed values of ND solid domain length scale (X_i^*) during the onset of solidification.

The second case study involves predicting the cooling curve for intended constant interface growth rate of 100 $\mu m/s$, when shrinkage effect is taken into account. The second validation is obtained through comparing the inputs and solutions of the inverse and the forward problems. Densities of solid and liquid phases of pure Al is considered to be $\rho_s = 2550\ kg/m^3$ and $\rho_l = 2250\ kg/m^3$. Rest of the thermophysical properties, initial length of the melt sample, and initial temperature of the domain are kept unchanged. The constant cooling rate of the bottom boundary prior to the onset of solidification is maintained at $C_r = 0.02\ K/s$.

In figure 3.2(a), the solid line shows the cooling curve obtained during solidification of pure Al with prescribed growth rate of 100 $\mu m/s$, when shrinkage effect is considered. This cooling curve is obtained from the proposed inverse model considering shrinkage effect. The cooling curve shown by dashed line in figure 3.2(a) corresponds to the no-shrinkage condition. It is evident from figure 3.2(a), that complete solidification of the domain is achieved faster, when shrinkage effect is considered. This result is physically consistent. The cooling curve addressing shrinkage effect (solid line in figure 3.2(a)) is used as the boundary condition for the forward model to evaluate the time evolution of crystal growth rate. Figure 3.2(b) shows the time evolution of crystal growth rate. The agreement between the predicted interface velocity and intended interface velocity is found out to be excellent (error limit is within 1 %). For the forward problem, length scale of the solid domain at the onset of solidification is unknown. One of the obvious choice of this initial length scale can be directly calculated based on intended crystal growth rate (for $\Delta t^{(1)} = 0.05\ s$, $x_i = \Delta t^{(1)} v_i = 5\ \mu m$ and $X_i^* = 0.00005$). However, to check the robustness of the method, three different values of X_i^* (initial non dimensional length of solid region) are assumed during onset of solidification. From figure 3.2(b) it can be observed that all these initial length assumptions converge to the intended interface velocity with 99 % accuracy. The small error in forward calculation of the interface growth rate can be attributed to the time averaged treatment of cold boundary temperature for individual time steps, and, numerical errors associated with the implementation of the semi-analytical scheme.

Experimental study of unidirectional solidification inherently accounts for the shrinkage effect. The models derived from the theory may, or, may not address shrinkage effect. The predicted cooling curves ($T_c(0,t)$) in figure 3.2(a) have different gradients on the basis of shrinkage and no shrinkage assumptions in the model. For both of these assumptions, we have considered the same crystal growth rate of 100 $\mu m/s$, and same initial melt sample length of 100 mm. For

pure Al the shrinkage coefficient is defined as $\rho_l/\rho_s \approx 0.882$. Due to shrinkage, 100 mm long melt sample should ideally reduce to 88.2 mm solid, once the complete solidification of the sample is achieved. With a crystal growth rate of 100 $\mu m/s$, the complete solidification of 100 mm melt sample, after onset of solidification, should be achieved during a time duration of 882 s (solid line in figure. 3.2(a)) whereas, if we ignore shrinkage, 100 mm long melt sample will turn into 100 mm long solid after solidification during a period of 1000 s (dashed line in figure 3.2(a)). Therefore, cooling rate (K/s) obtained from the shrinkage model is larger than the cooling rate predicted by no-shrinkage model. Usage of the cooling curve ($T_c(0,t)$) obtained from no-shrinkage model to a real experiment will cause a slower crystal growth rate as compared to the desired value. If we do not account for the shrinkage effect in the model to predict $T_c(0,t)$, the mismatch in experimentally obtained directional crystal growth rate from the desired value will keep increasing with decreasing ρ_l/ρ_s value.

The third case study is associated with prediction of cooling curve, when the desired unidirectional crystal growth rate varies with time ($v_i = f(t)$). The accuracy of the predicted $T_c(0,t)$ from the proposed model is scrutinized for time varying crystal growth rate condition. To begin with, a time varying crystal growth rate is obtained in the following manner. (i) The temperature at the bottom cold boundary of the melt sample is brought down to freezing point temperature (T_m) from its initial temperature (T_i) with a cooling rate of $C_r = 0.02\ K/s$. (ii) Once the bottom boundary reaches (T_m), a constant heat flux (heat flux removal rate q'' = 102250 W/m^2) condition is applied at this boundary. (iii) For this constant heat flux boundary condition, time dependent crystal growth rate ($dx_i/dt = v_i(t)$), and temperature history at the bottom of the sample (cooling curve $T_c(0,t)$) are evaluated.

The third validation involves using this time dependent crystal growth rate (obtained from constant heat flux boundary condition) as the input to the inverse problem to evaluate the cooling curve ($T(0,t) = T_c(0,t)$). The cooling curve obtained from the inverse model is compared with the original $T_c(0,t)$ evaluated from the constant heat flux (heat removal) boundary condition.

The cooling curve ($T_c(0,t)$) obtained from the inverse model is also cross verified in the following manner. (i) $T_c(0,t)$ obtained by solving the inverse problem is used as the boundary condition for the forward problem to evaluate time varying crystal growth rate ($v_i(t)$). (ii) Time evolution of crystal growth rate ($v_i(t)$) from the forward model is compared with the original $v_i(t)$ evaluated from the constant heat flux (heat removal) boundary condition.

The solution of Eq. 2.1-2.3 after the onset of solidification with constant heat flux (heat removal) boundary condition are given as follows Ozisik [2002]:

$$T_s = \frac{q''(x - x_i^{(k)})}{k_s} + T_m + \sum_{n=1}^{\infty} \exp\left(\frac{-\alpha_s(2n-1)^2\pi^2\Delta t^{(k)}}{4{x_i^{(k)}}^2}\right) \cos\left(\frac{(2n-1)\pi x}{2x_i^{(k)}}\right) C_n^{(k)} \tag{3.20}$$

$$T_l = T_m + \sum_{n=1}^{\infty} \exp\left(\frac{-\alpha_l(2n-1)^2\pi^2\Delta t^{(k)}}{4(L^{(k)} - x_i^{(k)})^2}\right) \sin\left(\frac{(2n-1)\pi(x - x_i^{(k)})}{2(L^{(k)} - x_i^{(k)})}\right) D_n^{(k)} \tag{3.21}$$

with,

$$C_n^{(k)} = \exp\left(\frac{-\alpha_s(2n-1)^2\pi^2\Delta t^{(k)}}{4{x_i^{(k-1)}}^2}\right) C_n^{(k-1)} \tag{3.22}$$

$$D_n^{(k)} = \exp\left(\frac{-\alpha_l(2n-1)^2\pi^2\Delta t^{(k)}}{4(L^{(k)} - x_i^{(k)})^2}\right) D_n^{(k-1)} \tag{3.23}$$

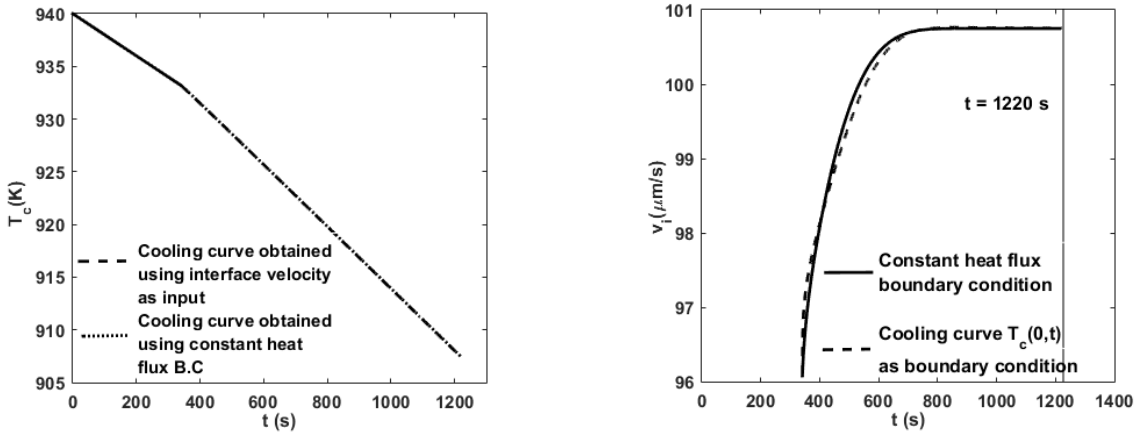

(a) (b)

Figure 3.3 : (a) Comparison between cooling curves ($T_c(0,t)$) obtained from the proposed inverse model and the forward model with constant heat flux boundary condition, and (b) comparison of interface velocities ($v_i(t)$) obtained from the forward models with $T_c(0,t)$ and constant heat flux boundary conditions.

where $C_n^{(1)} = 0$ and $D_n^{(1)}$ can be calculated from Eq. 3.9 by replacing all the ND parameters with dimensional parameters (replace X, X_i^*, L^*, θ_l, θ_m with x, x_i, L, T_l, T_m respectively).

Figure 3.3(a) shows the comparison between the cooling curves ($T_c(0,t)$) predicted from the proposed inverse model and forward model (Eq. 3.20) with constant heat flux boundary condition. Crystal growth rate ($v_i(t)$ shown in figure 3.3(b) with the solid line) predicted by the forward model (Eq. 3.20-3.23, and Eq. 2.2) with constant heat flux boundary condition is used as the input to solve the inverse problem. The comparison shown in figure 3.3(a) furnishes extremely good agreement between the two cooling curves.

The cooling curve ($T_c(0,t)$) obtained from the inverse model (dashed line in figure 3.3(a)) is then used as the boundary condition (Dirichlet type boundary condition) to the forward model to recalculate $v_i(t)$. Figure 3.3(b) shows the comparison between the crystal growth rates (v_i) obtained from forward models with cooling curve ($T_c(0,t)$) and constant heat flux boundary conditions respectively. Once again, the agreement between the two predictions is found out to be excellent. The small difference between the results shown in figure 3.3(b) can be attributed to the time averaged treatment of cold boundary temperature for individual time steps (for $T_c(0,t)$ boundary condition), and, numerical errors associated with the implementation of the semi-analytical scheme.

The fourth and the final case study provides the most significant validation of the proposed model, since it involves comparison of the inverse model prediction with the experimental data. An experimental setup similar to the present study (figure 2.1) involving unidirectional solidification of pure Al and Al-Si alloy is reported by Gandin [2000b,a]. Properties of 99.99 wt% pure Al are considered ($\rho_s = 2535\ kg/m^3$, $\rho_l = 2370\ kg/m^3$, $k_l = 90\ W/mK$, $k_s = 210\ W/mK$, $c_{ps} = 1183\ J/kgK$, $c_{pl} = 1087\ J/kgK$, $h_{sl} = 398\ kJ/kg$, and $T_m = 933.04\ K$ [Gandin, 2000b]).

A melt sample of 119 *mm* length is initially maintained at an uniform temperature of 1030.84 *K* [Gandin, 2000b]. Unidirectional solidification in the melt sample is achieved by heat removal from the bottom [Gandin, 2000b]. During the solidification process, temperature was continuously monitored at different locations of the solidifying melt sample, and local cooling curves at the thermocouple locations were plotted. Seven thermocouples were placed at an interval of 20 *mm* starting from the bottom of the melt sample. Average interface velocity was estimated

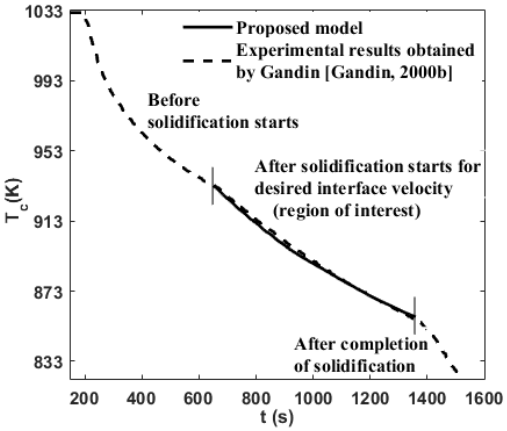

Figure 3.4 : Comparison of predicted cooling curves obtained from the proposed model and thermocouple data (thermocouple data at a distance of 60 *mm* from the bottom chiller) by Gandin [2000b].

by recording the time delay of attaining the freezing temperature at successive thermocouple locations. The interface velocity was also evaluated by using a one dimensional heat flow model. The interface velocities obtained from experimental measurement and semi-analytical solution showed reasonable agreement.

For the present validation, average interface velocity, estimated by Gandin [2000b] (in figure 5(b) of Gandin [2000b] with adiabatic boundary condition), is used as the input to the proposed inverse model. The cooling curve ($T_c(t)$) at the third thermocouple location [Gandin, 2000b] is predicted. The third thermocouple is located at a distance of 60 *mm* from the water cooled copper chill in the original experiment [Gandin, 2000b]. The cold bottom boundary for the proposed inverse model is chosen to coincide with the third thermocouple location in the original experiment [Gandin, 2000b]. In our proposed model, the cooling of the bottom boundary from the initial temperature (1030.84 *K*) to the freezing point ($T_m = 933.04$ *K*) replicates the cooling curve data from the third thermocouple location (from figure 3 by Gandin [2000b]). During this initial cooling process (till $T_c(0,t) = T_m$), the temperature distribution in the sample melt is obtained using forward model (Well defined boundary condition). Once the bottom boundary attains freezing point temperature, the interface velocity data, estimated by Gandin [2000b] (from figure 5.b by Gandin [2000b]), is used as the input to the proposed inverse model for evaluating $T_c(0,t)$.

Figure 3.4 shows the comparison between the cooling curves obtained from the proposed inverse model, and, thermocouple data reported by Gandin [2000b] (the dark solid line and dash-dot line framed within the vertical bars in figure 3.4). The comparison shown in figure 3.4 furnishes fairly good agreement (maximum absolute error: 2.85 *K*). Therefore, the reliability and robustness of the proposed model are conclusively ascertained.

3.4 SUMMARY

A 1-D semi-analytical transient heat diffusion model is developed, which is capable of predicting cooling curves for desired unidirectional crystal growth rate during solidification of pure or eutectic materials. The shrinkage effect is incorporated in the proposed model. Four different case studies are performed to validate the proposed model. The first case study validates the proposed model with existing enthalpy updating scheme based numerical model. The second case study is validated by solving inverse and forward problems associated with constant crystal growth rate. The third case study involves prediction and validation of cooling curve for time varying crystal growth rate. The fourth and the most crucial validation of the proposed model is presented by comparison between cooling curves obtained from the model prediction and

experimentally measured data. Shrinkage during solidification is considered for all the validating case studies except the first one. All the case studies produced remarkably good validation (with maximum error limit within 1.5 %), ascertaining the reliability and robustness of the proposed model. The proposed model will be rendered beneficial to obtain prior knowledge of cooling curves for controlled crystal growth rate.

…